Available online at www.sciencedirect.com

SciVerse ScienceDirect

Ceramics International 38 (2012) 4623–4630

CERAMICS INTERNATIONAL

www.elsevier.com/locate/ceramint

Effect of heterojunction on photocatalytic properties of multilayered ZnO-based thin films

Nasrin Talebian [a,*], Mohammad Reza Nilforoushan [b], Zahra Salehi [a]

[a] *Department of Chemistry, Shahreza branch, Islamic Azad University, Razi Chemistry Resreach Centre, Women Research Council, 86145-311 Shahreza, Isfahan, Iran*

[b] *Engineering Department, Sharekord University, Sharekord P.B. 115, Iran*

Received 17 August 2011; received in revised form 20 January 2012; accepted 13 February 2012
Available online 21 February 2012

Abstract

In the present study, the effects of the heterojunctions on the optical and structural characteristics and the resulting photocatalytic properties of multilayered ZnO-based thin films were investigated. The junctions were composed of semiconducting ZnO nano-porous films coated on the In_2O_3 and SnO_2 counterpart layers. The multilayered ZnO films based on the triple-layered Ag-doped indium oxide (AIO)/tin oxide (TO)/zinc oxide (ZnO), indium oxide (IO)/Ag-doped tin oxide (ATO)/zinc oxide (ZnO), indium oxide (IO)/tin oxide (TO)/zinc oxide (ZnO) and tin oxide (TO)/indium oxide (IO)/zinc oxide (ZnO) have been fabricated by subsequent sol–gel dip coating. Their structural and optical properties combined with photocatalytic characteristics were examined toward degradation of Solantine Brown BRL (C.I. Direct Brown), an azo dye using in Iran textile industries as organic model under UV light irradiation. Effects of operational parameters such as initial concentration of azo dye, irradiation time, solution pH, absence and presence of Ag doping and consequent of sublayers on the photodegradation efficiencies of ZnO nultilayered thin films were also investigated and optimum conditions were established. It was found that the photocatalytic degradation of azo dye on the composite films followed pseudo-first order kinetics. Photocatalytic activity of AIO/TO/ZnO interface composite film was higher compared with other films and the following order was observed for films activities: AIO/TO/ZnO > IO/TO/ZnO > ATO/IO/ZnO > TO/IO/ZnO. Differences in the film efficiencies can be attributed to differences in crystallinity, interfacial lattice mismatch, and surface morphology. Besides, the presence of Ag doping between layers that may act as trap for electrons generated in the ZnO over layer thus preventing electron–hole recombination.
© 2012 Elsevier Ltd and Techna Group S.r.l. All rights reserved.

Keywords: A. Sol–gel processes; B. Interfaces; B. Composites; B. Spectroscopy; C. Optical properties

1. Introduction

Transparent semi-conducting oxide thin films of In_2O_3, SnO_2, ZnO and their mixtures have been extensively used in optoelectronic applications such as transparent electrodes in touch panels, at panel displays (FPD), and other devices [1–7]. Besides, multilayered transparent conducting films, consisting of thin films of Ag or Ag alloys sandwiched between transparent conducting oxide films such as indium–tin oxide, tin oxide and zinc oxide have been extensively studied for applications such as transparent conducting electrodes in flat-panel displays, low-emissivity coatings in architectural glasses and electromagnetic interference (EMI) shielding of plasma display panel (PDP) [8–16]. Many of the previous works on the multilayered transparent conducting films were focused on the opto-electronic applications [8–12], and a few studies on the photocatalytic properties of such coatings [17–22].

Multilayer thin films show different physical properties other than the conventional monolayer thin films [23]. The quality of films deposited on buffer layer is found to be superior to those grown directly on a substrate [23–25]. In recent years, a great deal of interests has been devoted to the photocatalytic degradation of organic water pollutants by semiconductor particles. Textile dyes are of environmental interest because of their widespread use and their potential for forming toxic aromatic amines. Among the synthetic dyes, which are widely used for textile dyeing and other industrial applications, those containing an azo chromophore constitute the largest class [26]. Azo dyes are a class of dyes, which are widely used in a variety

* Corresponding author. Tel.: +98 321 329 2260; fax: +98 321 3232701.
E-mail addresses: nasrin_talebian@yahoo.com, talebian@iaush.ac.ir (N. Talebian).

0272-8842/$36.00 © 2012 Elsevier Ltd and Techna Group S.r.l. All rights reserved.
doi:10.1016/j.ceramint.2012.02.042

of products, such as textiles, paper, foodstuffs or leather. However, these compounds and degradation products can be hazardous because their toxicity and carcinogenicity [27]. Excess use of various dyes in the textile industry has led to the severe surface water and groundwater contamination by releasing the toxic and colored effluents [28]. It is important for the sake of increasing amount, its variety and resistance to biological destruction [29].

Many dye pollutants can be degraded effectively and ultimately mineralized using Advanced Oxidation Processes'' (AOP). Among these processes, heterogeneous photocatalys is was found as an emerging destructive technology leading to the total mineralization of most of organic pollutants [30–32]. In most cases, the degradation is conducted for dissolved compounds in water with UV-illuminated TiO_2 powder and thin film. Recently, much effort has been devoted to study ZnO as a very promising photocatalyst for photocatalytic degradation of water pollutants [33–36].

Besides, there is still drawback associated with its use: charge carrier recombination occurs within nanoseconds. Some variety of systems, including ZnO/semiconductor coupled systems,coupling of two or more semiconductors with appropriate energy levels, and a few ones including metal-loaded ZnO systems and ZnO based multilayered films were introduced to solve this problem [37,38].

An increase of the lifetime of photogenerated electron–hole pairs in the multi-component oxides, due to the hole and electron transfer between the interfaces of the composite films, is crucial to the catalytic activity enhancement in multilayered systems. Nevertheless, it should be considered that the photocatalyitc activity also strongly depends on the proposed compatibilities of multi-layer oxide films. Therefore, the choice of substrate materials is governed by the requirement for lattice matching and preferential growth along certain crystallographic direction.

We report here the influence of Ag doped (In_2O_3–SnO_2)/ZnO heterojunction multi-layers on the microstructure as well as the optical properties and photocatalytic activity of ZnO thin films prepared using sol–gel procedure. These properties were compared with the single layer ZnO thin film.

2. Material and methods

2.1. (In_2O_3–SnO_2)/ZnO multilayer thin films preparation

All the chemical reagents used in our experiments were of analytical grade and used without further purification. Thin films based on (In_2O_3–SnO_2)/ZnO triple-layered structures were prepared on glass substrate by subsequent sol–gel dip coating of sol solution of individual metal precursor. The sols were prepared using zinc acetate dehydrate ($Zn(Ac)_2{\cdot}2H_2O$), hydrated stannic chloride ($SnCl_4{\cdot}5H_2O$), hydrated indium chloride ($InCl_3{\cdot}4H_2O$) separately as sources of In, Sn and Zn, respectively, and absolute ethanol as solvent. One of the sets including In and Sn precursors was left unmixed to prepare undoped films, while in the remaining sets, requisite amounts of silver nitrate dissolved in acetonitrile was added to obtain sols with 1:10 Ag–Sn and Ag–In molar ratio. The sols were continuously stirred at room temperature till clear sols devoid of any precipitates or particulates were obtained. The sol samples were then heated on hot plate with continuous stirring until the solution becomes gel like. Glass substrates were dipped in the starting solutions in a way that five different samples of multilayered ZnO films based on the triple-layered Ag-doped indium oxide (AIO)/tin oxide (TO)/zinc oxide (ZnO), indium oxide (IO)/Ag-doped tin oxide (ATO)/zinc oxide (ZnO), indium oxide (IO)/tin oxide (TO)/zinc oxide (ZnO) and tin oxide (TO)/indium oxide (IO)/zinc oxide (ZnO) have been fabricated by subsequent sol–gel dip coating. The deposited layers were then dried in air at 250 °C for 15 min after each dipping. The crystallization of the last deposited layer of the same component was finally performed by thermal annealing in air at temperature of 500 °C for 60 min after three coating cycles.

2.2. Structural and morphological characterization

To characterize (In_2O_3–SnO_2)/ZnO multilayered films, X-ray power diffraction (XRD) experiments were performed on a Bruker, D8 ADVANCE XRD diffraction spectrometer with a Cu Kα line at 1.5406 Å and a Ni filter for an angle range of $2\theta = 5$–100°. Philips, XL30 scanning electron microscope (SEM) measurements were also used to investigate the morphology of the samples with an accelerating voltage of 17 kV. The optical properties were obtained by UV–vis absorption measurement.

2.3. Azo dye photodegradation

The obtained films were placed inside 50 mL of azo solution filled in a cylinder quartz vessel and illuminated with four 8 W UV lamps (Philips UV-C, λ = 365 nm). The distance between the UV source and solution was 12 cm. At given time intervals, samples were withdrawn from test solution and analyzed by measuring the absorbance at 435 nm with a spectrophotometer. Consequently, the degradation rate for azo could be calculated according to the change in the absorbance. In the photocatalytic experiments, five samples were used to investigate the effects of initial azo dye concentration and pH on the photocatalytic activity.

3. Results and discussions

3.1. Structural characterization of multilayered ZnO-based films

In order to understand the influence of the various layered structures, several types of film were produced and characterized. The crystallinity and the preferred crystal orientation of all films were analyzed by the X-ray diffraction (XRD) method. Fig. 1 shows the X-ray diffraction patterns of five samples including multilayered AIO/TO/ZnO, IO/TO/ZnO, ATO/IO/ZnO and TO/IO/ZnO thin films and single layer ZnO thin film.

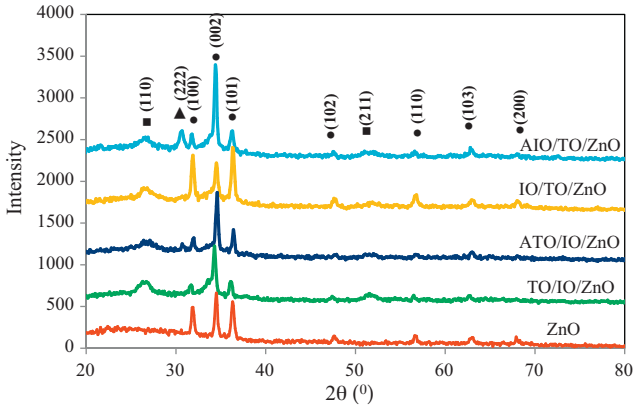

Fig. 1. XRD patterns of samples indicating the rutile phase of SnO_2 (■), the wurtzite phase of ZnO (▲) and cubic phase of In_2O_3 (●).

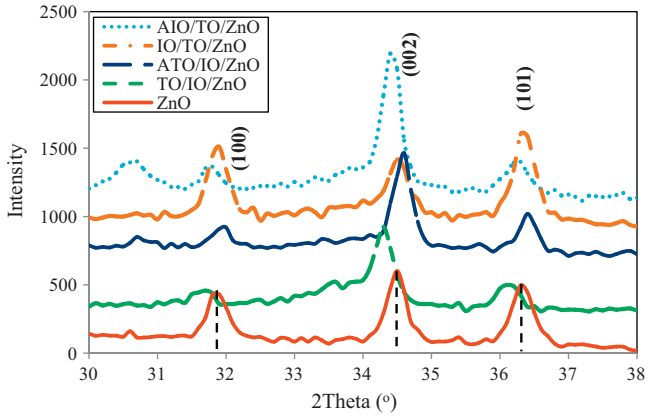

Fig. 2. Comparison of (1 0 0), (0 0 2), and (1 0 1) peaks from the XRD pattern of ZnO-based samples.

All main diffraction peaks can be attributed to crystalline ZnO with the hexagonal wurtzite structure. The data are in agreement with the Joint Committee on Powder Diffraction Standards (JCPDS) card for ZnO (JCPDS 036-1451). Moreover, the peak intensities of the ZnO features are found to vary with the composition of the nanostructures. For IO/TO/ZnO film, the (1 0 1) and (1 0 0) ZnO peaks appear to be more intense, indicating their preferred growth directions. The relative intensity of the (0 0 2) ZnO peak is found to increase for AIO/TO/ZnO, ATO/IO/ZnO and TO/IO/ZnO, respectively, suggesting the beginning of the *c*-axis oriented growth. However, due to the random growth direction of the ZnO nanoparticles, other peaks are also present.

At the same time it is also evident that the characteristic diffraction (2 2 2) peak of In_2O_3 (44-1087 JCPDS) card with a cubic lattice structure appear in the XRD patterns of the Ag doped samples and it is absent in undoped ones, which suggests that the Ag doping improved crystal growth in the multilayered ZnO-based films. Ag doped films have a polycrystalline structure dominantly grown in the preferred crystal planes such as (1 1 0) for SnO_2, (2 2 2) for In_2O_3, and (1 0 0), (0 0 2), (1 0 1) for ZnO.

To study the effect of doping and interfacial lattice mismatch on the crystallinity of the ZnO nanostructures, the intensity of the (1 0 0), (0 0 2), and (1 0 1) diffraction peaks was monitored. The intensity of the diffraction peaks (1 0 0) and (1 0 1) and their full width at half-maximum (FWHM) decreased, for Ag-doped samples (see Fig. 2 and Table 1). The mean size of nano-particles was estimated by Scherer's equation [39] and reported in Table 1. As seen, the grain size of nanoparticles in Ag doped films improved. Such changes in crystallinity might be the result of changes in the atomic environment due to impurity doping on In_2O_3 and SnO_2 sublayers.

There was also a small shift to a higher 2θ angle value of (0 0 2) peak for AIO/TO/ZnO and IO/TO/ZnO films as compared with single layer ZnO. For ATO/IO/ZnO and TO/IO/ZnO films, more shifts were observed to higher and lower angles, respectively.

Structurally, tin oxide crystallizes in a tetragonal structure ($P4_2/mnm$, $a = 3.249$ Å and $c = 5.206$ Å), while zinc oxide is hexagonal, crystallizing in the wurtzite structure ($P6_3mc$, $a = 4.737$ Å and $c = 3.186$ Å) and indium oxide is cubic (m3m, $a = 10.12$ Å) [40–42]. Hence, the lattice mismatch between ZnO and In_2O_3 is larger than between ZnO and SnO_2, so in the growth of ZnO/In_2O_3 heterostructures, many misfit dislocations exist in order to release the strain. This produces disorders dominantly through an increase in the grain boundary density and thereby decreases the crystallite size as shown in Table 1 [43]. The different lattice mismatch between the ZnO and SnO_2 and In_2O_3 substrate induces strains of various kinds with varying degrees. As observed from XRD data in Table 1, a larger lattice deformation was observed for ATO/IO/ZnO and TO/IO/ZnO films due to larger interfacial lattice mismatch between In_2O_3 and ZnO.

3.2. Morphological characterization of multilayered ZnO-based films

Fig. 3 shows the scanning electron microscopy (SEM) images of five different ZnO nanostructures grown on different substrates. We can see clearly the influence of incorporation of Ag on the surface morphology of multilayered ZnO films. Besides, Ag doping results to improvement of crystallinity. The

Table 1
XRD parameters obtained for (0 0 2) diffraction peak.

	Standard powder	AIO/TO/ZnO	IO/TO/ZnO	ATO/IO/ZnO	TO/IO/ZnO	ZnO
2θ	34.438	34.447	34.541	34.594	34.283	34.441
c	5.2070	5.1834	5.1936	5.1848	5.2239	5.2001
FWHM	–	0.312	0.345	0.370	0.383	0.425
Mean size (nm)	–	96	78	58	52	42

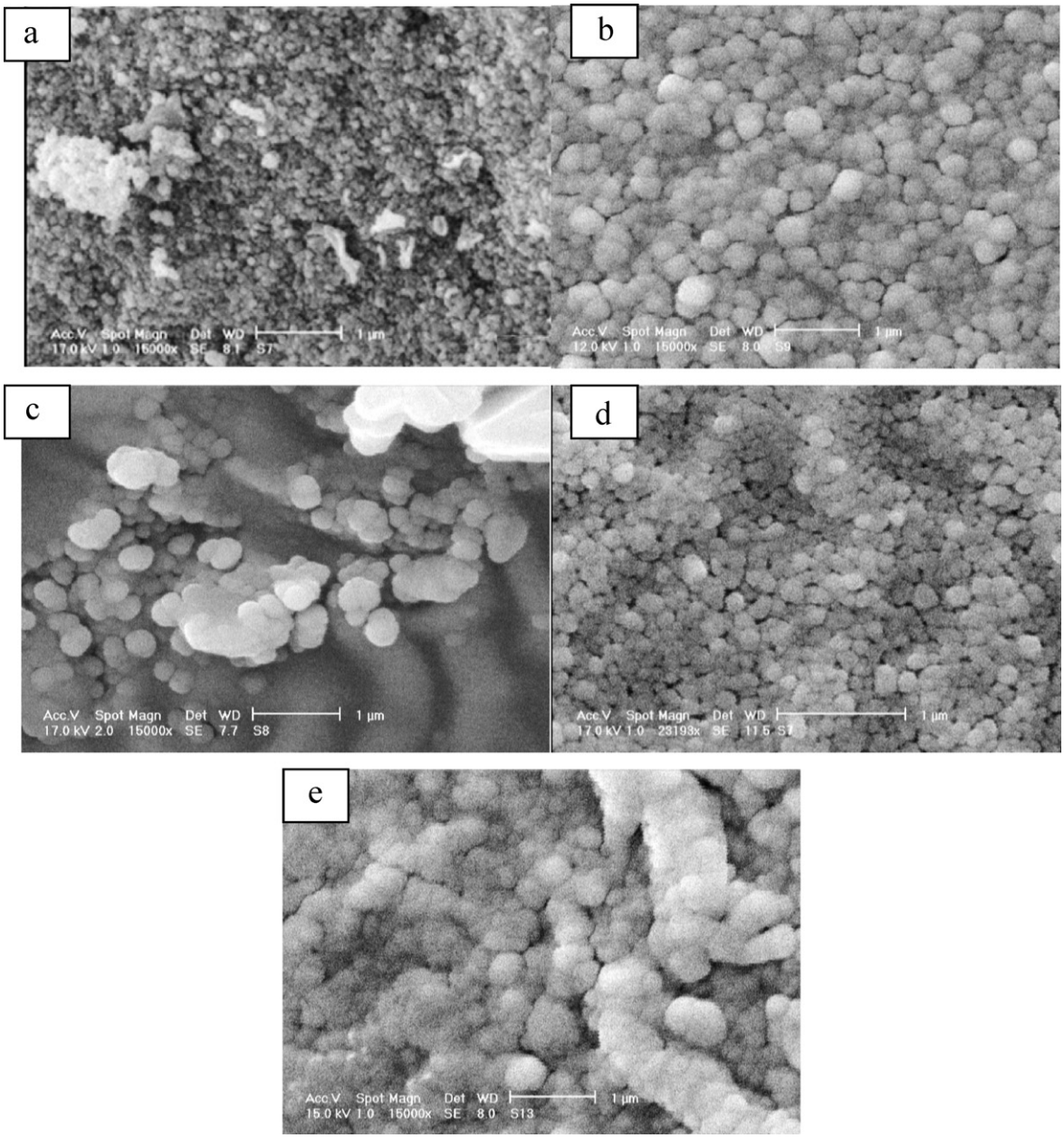

Fig. 3. SEM images of (a) ZnO, (b) AIO/TO/ZnO, (c) IO/TO/ZnO, (d) ATO/IO/ZnO and (e) TO/IO/ZnO.

agglomeration of nano-particles occuring in the case of undoped was not obvious for the AIO/TO/ZnO and ATO/IO/ZnO films and some micro cracks are observed in later films. ZnO particles are better distributed on Ag doped underlying surface than on undoped surface. This may favor the absorption of irradiation light by semiconductors.

3.3. Optical characterization of multilayered ZnO-based films

The optical properties of ZnO nanostructures were examined by using UV–vis spectroscopy. The fundamental absorption edge of the films corresponds to electron transitions from valence band to conduction band and this edge can be used to calculate the optical band gap of the films. The energies of absorption edges were determined by extrapolating the horizontal and sharply rising portions of the curve and defining the edge as the energy of the intersection. The band gap energies (E_g) calculated on the basis of the corresponding absorption edges are shown in Fig. 4. As seen from Fig. 3, E_g values of ZnO films varies from 3.15, 3.28, 3.39, 3.33 to 3.52 eV for ZnO, TO/IO/ZnO, ATO/IO/ZnO, IO/TO/ZnO and AIO/TO/ZnO, respectively. The absorption edge is blue shifted for Ag doped films; this may be attributed to improved crystalline quality of the ZnO films. An increase in band-gap energy of a semiconductor, resulting in the valance band potential becoming more positive and conduction band potential more negative. It is anticipated that AIO/TO/ZnO film should show a higher photocatalytic activity than other films. The blue shift can be explained by the charge transfer

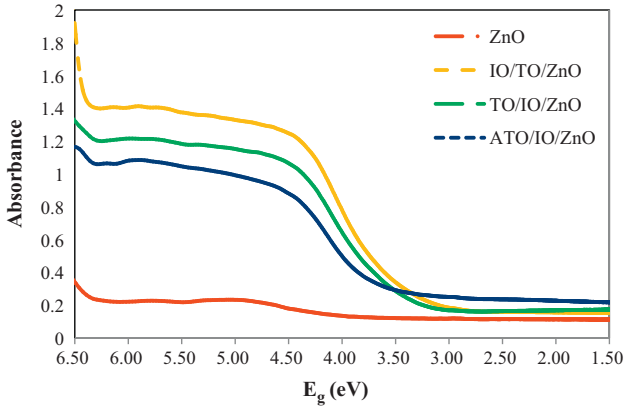

Fig. 4. UV–vis diffuse reflectance absorption spectra of the samples.

occuring between the interfaces of the composite films [44]. Because the conduction band energy levels of SnO_2 match with those of ZnO, the photogenerated electrons from ZnO are quickly injected into the conduction band of SnO_2 while the holes remain on the ZnO. The transferred electrons will occupy the lower conduction band energy levels of SnO_2, the photons with higher energy absorbed for electrons, leading to a blue shift of absorption.

3.4. Evaluation of photocatalytic activity

The photodegradation of Solantine Brown BRL as an azo dye in water was used to evaluate the catalytic activity of the five prepared catalysts. Two experiments were run for each type of sample to investigate the effects of initial azo dye concentration, and solution pH on the photocatalytic activity. The activities of the different ZnO-based photocatalysts were evaluated by monitoring the UV–vis spectrum of irradiated azo solution at λ_{max} = 435 nm.

Fig. 5 shows a typical time-dependent UV–vis spectrum of azo dye solution during photoirradiation. The absorption peaks corresponding to the dye diminished and finally disappear under reaction, indicating the degradation of the dye. No new absorption bands appear in either the visible or ultraviolet regions, especially absorption bands of aromatic moieties or other similar intermediates.

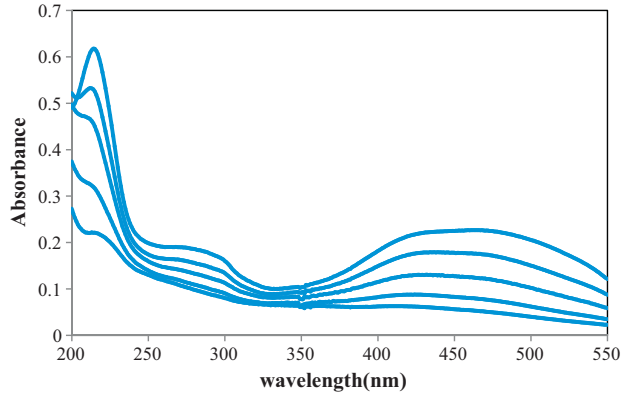

Fig. 5. Spectral changes during photocatalytic degradation of aqueous solution of azo dye after time interval of 10 min: pH = 9.0; AIO/TO/ZnO as catalyst and C_0 = 5 ppm.

3.4.1. Kinetic studies

Kinetic modeling of the photocatalytic process is usually restricted to the analysis of the initial rate of photocatalytic degradation. The kinetic and empirical equations, including the zero, first, Elovich and second order rate equations were applied to the azo dye removal efficiency with respect to time. The fitness of different kinetic equations to linear forms was evaluated based on the R^2.

$$\text{Zero order } [A] = [A]_o - kt \quad (1)$$

$$\text{First order } \ln[A] = \ln[A]_o - kt \quad (2)$$

$$\text{Second order } \frac{1}{[A]} = \frac{1}{[A]_o} + kt \quad (3)$$

$$\text{Elovich } q_t = \left(\frac{1}{\beta}\right)\ln\left(\frac{\alpha}{\beta}\right) + \left(\frac{1}{\beta}\right)\ln t \quad (4)$$

where q_t is amount of sorbate per unit mass of sorbent at time t. $\alpha$and $\beta$are empirical constants. Slope and intercept are $1/\beta$ and $(1/\beta)$ $\ln(\alpha/\beta)$, respectively. Based on kinetic data shown in Fig. 6, first order model is showing the highest R^2 value compared to other kinetic reaction models.

3.4.2. Effect of catalyats

It can be seen from Fig. 7 that ZnO showed very low photocatalytic activity and AIO/TO/ZnO showed highest photocatalytic activity. The rate constants obtained from the slop of plot $\ln(C_o/C)$ versus time are 0.085, 0.042, 0.036, 0.030 and 0.018 for AIO/TO/ZnO, IO/TO/ZnO, ATO/IO/ZnO, TO/IO/ZnO and ZnO, respectively.

The increase in photocatalytic activity of AIO/TO/ZnO film may attribute to the increase in band-gap energy of ZnO and to the effects of particle size and crystallinity. From the energy band structures and the relative positions of conduction band and valance band of In_2O_3–ZnO–SnO_2 heterojunction, it could be found that the photoinduced electron–hole pair separation occur in ZnO films with SnO_2 sublayer more extensive than ZnO films with In_2O_3 sublayer. It had been reported that the electron affinity of ZnO (χZnO) and SnO_2 (χSnO_2) was 4.3 and 4.5 eV, respectively; the band gap of ZnO (E_gZnO) was around 3.37 eV, and its work function (WZnO) was about 5.2 eV; the band gap of SnO_2 (E_gSnO_2) was around 3.5 eV, and its work function ($WSnO_2$) was about 0.3 eV smaller than that of ZnO [45–47]. The Fermi energy level of SnO_2 was higher than that of ZnO due to its smaller work function. Accordingly, when ZnO and SnO_2 formed a heterojunction, the photogenerated electron transfer occurred from the CB of ZnO to the CB of SnO_2 and, conversely, the photogenerated hole transfer could take place from the VB of SnO_2 to the VB of ZnO, suggesting that the photogenerated electrons and holes were efficiently separated.

On the other hand, the final nanocrystal size could be tailored by the proposed compatibilities of multi-layer oxide films and doping. As shown from XRD and SEM resuls, AIO/TO/ZnO film exhibits highly crystallinity, resulting to higher photoactivity. The crystal defect concentration associated to

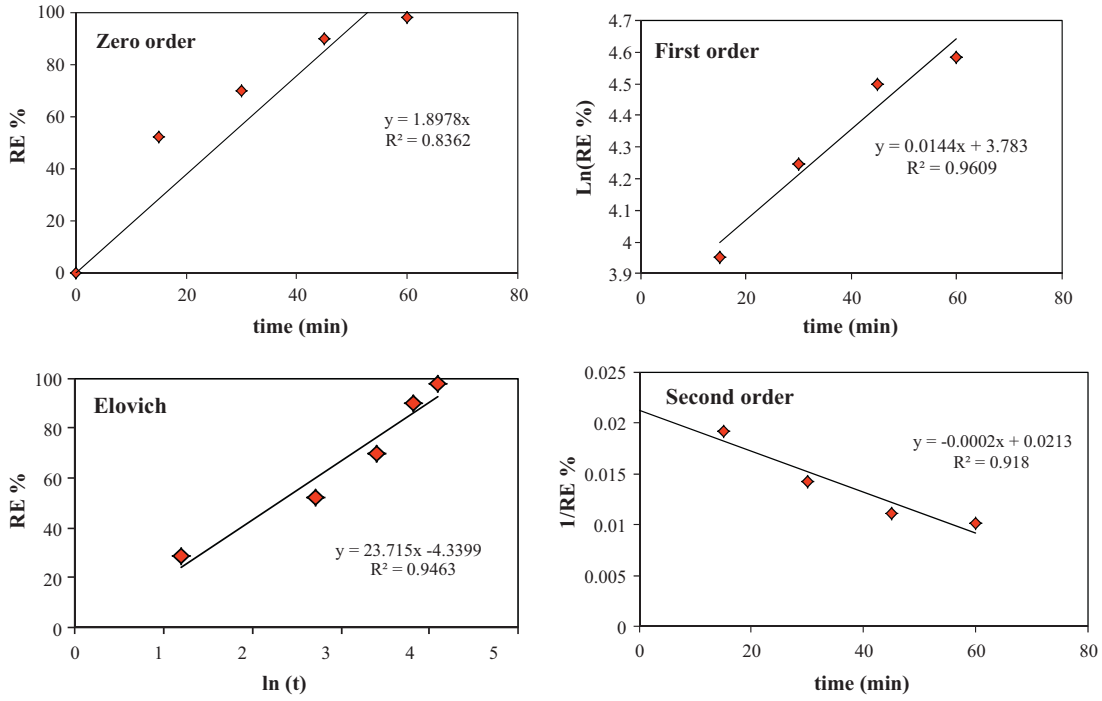

Fig. 6. Kinetic models of azo dye photodegradation on AIO/TO/ZnO as catalyst at pH = 9.0 and C_0 = 5 ppm.

trap states for the photogenerated carriers may be low in high quality nanocrystals, so that electron–hole separation can be maximized [48,49].

3.4.3. Effect of pH

The pH of solutions greatly affects the rate of reaction taking place on semiconductor surfaces due to its influences on surface-charge-properties of the photocatalysts. As shown in Fig. 8, the degradation efficiency for azo dye on ZnO-based films was pH-dependent in the pH range of 4–11.

For semiconductor the surface potential will be determined by reactions with the ions H^+ and OH^-. Thus, the surface potential is pH dependent. The pH where the particle is neutral is called PZC, point of zero charge. For pH > PZC the surface is negatively charged. For pH < PZC the surface is positively charged. It should be noted the pH_{pzc} of ZnO, SnO_2 and In_2O_3 are 8.80, 4.80 and 8.64, respectively [50]. The highest degradation rate was obtained at pH 4, 4, 7, 6, and 9 for ZnO, TO/IO/ZnO, ATO/IO/ZnO, IO/TO/ZnO and AIO/TO/ZnO, respectively. These results show not only morphology and optical properties but also the surface charge of multilayered ZnO-based films could be affected by sublayering structures. The ionization state of the surface of the photocatalyst under acidic and alkaline conditions and the nature of the pollutant to be degraded can be affected the amount of its adsorption on the catalysts surface and then the photodegradation efficiency.

3.4.4. Effect of concentration

From first-order kinetics, it can be found that the rate constants for degradation were inversely related to the dye concentrations. To understand whether dye photocatalytic degradation on multilayered ZnO composite films follows a

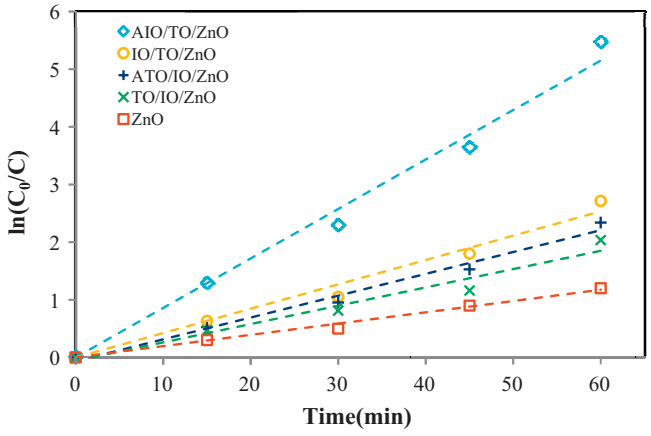

Fig. 7. Comparison for the photocatalytic activities of five catalysts after 60 min UV-irradiation.

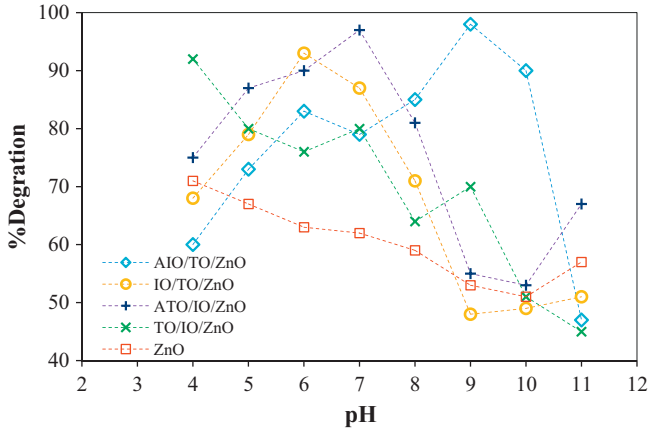

Fig. 8. Effect of pH on photocatalytic degradation of azo dye at initial concentration 5 ppm.

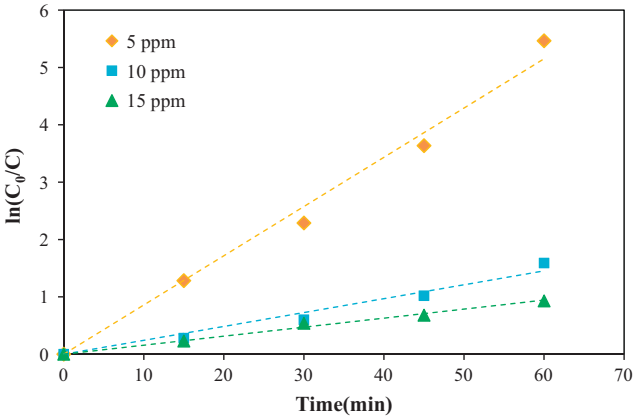

Fig. 9. Kinetic characters of photocatalytic degradation of azo dye at different initial concentrations.

Table 2
Kinetic parameters and linear coefficient R^2 for photocatalytic degradation of azo dye at different initial concentrations.

C_0 (mg/L)	k (min^{-1})	$t_{1/2}$ (min)	R^2
5	0.0858	11.65	0.9869
10	0.0242	28.64	0.9704
15	0.0157	44.15	0.9895

such kinetic model, photocatalytic experiments were carried out with azo solutions having concentrations of 5, 10, and 15 mg/L. Experimental data on $\ln(C_0/C_t)$ were plotted against t in Fig. 9. The kinetics parameters, rate constants (k) and half-life values ($t_{1/2} = 0.6932/k$) at different initial azo concentrations are given in Table 2. From first-order kinetics, it can be found that the rate constants for degradation were inversely related to the dye concentrations. This phenomenon can be explained as following reasons: as initial dye concentration increases, more adsorption of Solantine Brown BRL molecules onto the surface of catalyst hampers the competitive adsorption of OH^- and molecular oxygen, thus the generation of hydroxyl radicals and O_2^-as redox active oxygen species is reduced. Furthermore, the interception of photons from reaching to the catalyst surface results in the decreasing adsorption of photons by the catalyst, and consequently the degradation rate is reduced.

4. Conclusions

ZnO-based interface composite films with higher photocatalytic activities compared with single component ZnO film were successfully prepared by subsequent deposition of ZnO on the Ag doped and undoped In_2O_3 and SnO_2 counterpart layers. Their structural and optical properties combined with photocatalytic characteristics were examined toward degradation of Solantine Brown BRL (C.I. Direct Brown), an azo dye. Ag doped multilayered ZnO samples were highly polycrystalline, suggesting that the crystalline quality improved by doping. The photocatalytic activity was enhanced in the ZnO multi-layer structures by 1.7–4.7 order in comparison with the ZnO single-layer. Differences in the ZnO film efficiencies can be attributed to differences in crystallinity, interfacial lattice mismatch, and surface morphology as well as Ag doping. In summary, multilayer, multi-deposition technology sol–gel approaches to $In_2O_3/SnO_2/ZnO$ heterojunction layers show promising photocatalytic properties toward pollutants degradation.

Acknowledgement

The authors are grateful for the financial support provided by Islamic Azad University, Shahreza branch.

References

[1] C.A. Hoel, T.O. Mason, J.-F. Gaillard, K.R. Poeppelmeier, Transparent conducting oxides in the ZnO-In_2O_3-SnO_2 System, Chem. Mater. 22 (2010) 3569–3579.
[2] C.A. Hoel, J.M.G. Amores, E. Morn, M.A. lario-Franco, J.-F. Gaillard, K.R. Poeppelmeier, High-pressure synthesis and local structure of corundum-type $In_{2-2x}Zn_xSn_xO_3$ ($x \leq 0.7$), J. Am. Chem. Soc. 132 (2010) 16479–16487.
[3] M.-G. Kim, H.S. Kim, Y.-G. Ha, J. He, M.G. Kanatzidis, A. Facchetti, T.J. Marks, High-performance solution-processed amorphous zinc-indium-tin oxide thin-film transistors, J. Am. Chem. Soc. 132 (2010) 10352–10364.
[4] S.P. Harvey, K.R. Poeppelmeier, T.O. Mason, Subsolidus phase relationships in the ZnO–In_2O_3–SnO_2 system, J. Am. Ceram. Soc. 91 (2008) 3683–3689.
[5] J.H. Bae, J.M. Moon, S.W. Jeong, J.J. Kim, J.W. Kang, D.G. Kim, Transparent conducting indium zinc tin oxide anode for highly efficient phosphorescent organic light emitting diodes, J. Electrochem. Soc. 155 (2008) 1–6.
[6] M.S. Grover, P.A. Hersh, H.Q. Chiang, E.S. Kettenring, J.F. Wager, D.A. Keszler, Thin-film transistors with transparent amorphous zinc indium tin oxide channel layer, J. Phys. D: Appl. Phys. 40 (2007) 1335–1338.
[7] J. Ni, H. Yan, A.C. Wang, Y. Yang, C.L. Stern, A.W. Metz, MOCVD-derived highly transparent, conductive zinc- and tin-doped indium oxide thin films: precursor synthesis, metastable phase film growth and characterization, and application as anodes in polymer light-emitting diodes, J. Am. Chem. Soc. 127 (2005) 5613–5624.
[8] M. Bender, W. Seelig, C. Daube, H. Frankenberger, B. Ocker, J. Stollenwerk, Dependence of film composition and thicknesses on optical and electrical properties of ITO–metal–ITO multilayers, Thin Solid Films 326 (1998) 67–71.
[9] A. Köppel, W. Kriegseis, B.K. Meyer, A. Scharmann, C. Daube, J. Stollenwerk, J. Trube, Dependence of the electrical and optical behaviour of ITO-silver-TO multilayers on the silver properties, Thin Solid Films 365 (2000) 139–146.
[10] A. Köppel, B. Meyer, J. Trube, Influence of substrate temperature and sputtering atmosphere on electrical and optical properties of double silver layer systems, Thin Solid Films 392 (2001) 311–314.
[11] M. Farland, P. Karlsson, C. Charton, Low resisitivity transparent electrodes for displays on polymer substrates, Thin Solid Films 392 (2001) 334–337.
[12] K.H. Choi, Y.J. Kim, Y.S. Lee, H.J. Kim, ITO/Ag/ITO multilayer films for the application of a very low resistance transparent electrode, Thin Solid Films 341 (1999) 152–155.
[13] E. Ando, M. Miyazaki, Moisture resistance of the low-emissivity coatings with a layer structure of Al-doped ZnO/Ag/Al-doped ZnO, Thin Solid Films 392 (2001) 289–293.
[14] P. Sawunyama, A. Yasumori, K. Okada, The nature of multilayered TiO_2-based photocatalytic films prepared by a sol–gel process, Mater. Res. Bull. 33 (1998) 795–801.
[15] T. Okamura, F. Yamazaki, R. Oi, M. Yoshikai, M. Koyama, U.S. Patent No. 6104530, 15 August, 2000.
[16] S. Takaki, K. Sato, M. Miyazaki, Y. Kawamura, H. Nishimura, U.S. Patent No. 6221520, 24 April, 2001.

[17] R. Suárez-Parra, I. Hernández-Pérez, M.E. Rincón, S. López-Ayala, M.C. Roldán-Ahumad, Visible light-induced degradation of blue textile azo dye on TiO_2/CdO–ZnO coupled nanoporous films, Sol. Energy Mater. Sol. Cells 76 (2003) 189–199.
[18] X.-T. Wang, S.-H. Zhong, X.-F. Xiao, Photo-catalysis of ethane and carbon dioxide to produce hydrocarbon oxygenates over ZnO–TiO_2/SiO_2 catalyst, J. Mol. Catal. A: Chem. 229 (2005) 87–93.
[19] W. Shouqiang, S. Zhongcai, L. Xudong, L. Ying, C. Linlin, H. Yan, Photocatalytic degradation of methyl orange over ITO/CdS/ZnO interface composite films, J. Environ. Sci. 21 (2009) 991–996.
[20] X.-T. Wang, S.-H. Zhong, X.-F. Xiao, Photo-catalysis of ethane and carbon dioxide to produce hydrocarbon oxygenates over ZnO-TiO_2/SiO_2 catalyst, J. Mol. Catal. A: Chem. 229 (2005) 87–93.
[21] J. Shang, W.Q. Yao, Y.F. Zhu, N.Z. Wu, Structure and photocatalytic performances of glass/SnO_2/TiO_2 interface composite film, Appl. Catal. A: Gen. 257 (2004) 25–32.
[22] H.M. Yates, L.A. Brook, I.B. Ditta, P. Evansa, H.A. Foster, D.W. Sheel, A. Steele, Photo-induced self-cleaning and biocidal behavior of titania and copper oxide multilayers, J. Photochem. Photobiol. A 197 (2008) 197–205.
[23] R. Hong, J. Shao, H. He, Z. Fan, Enhancement of near band edge photoluminescence of ZnO thin films in sandwich configuration at room temperature, J. Appl. Phys. 99 (2006) 093520–093523.
[24] J. Herrero, C. Guillen, Improved ITO thin films for photovoltaic applications with a thin ZnO layer by sputtering, Thin Solid Films 451–452 (2004) 630–633.
[25] W.S. Choi, E.J. Kim, S.G. Seong, Y.S. Kim, C. Park, S.H. Hahn, Optical and structural properties of ZnO/TiO_2/ZnO multi-layers prepared via electron beam evaporation, Vacuum 83 (2009) 878–882.
[26] H. Zollinger, Colour Chemistry: Synthesis Properties and Applications of Organic Dyes and Pigments, Wiley-VCH, New York, 1987, pp. 92–102.
[27] E. Rindle, W.J. Troll, Metabolic reduction of benzidine. Azo dyes to benzidine in the rhesus monkey, Natl. Cancer Inst. 55 (1975) 181–187.
[28] I.A. Salem, M.S. El-Maazawi, Kinetics and mechanism of color removal of Methylene blue with hydrogen peroxide catalyzed by some supported alumina surfaces, Chemosphere 41 (2000) 1173–1180.
[29] M.R. Sohrabi, M. Ghavamia, Photocatalytic degradation of Direct Red 23 dye using UV/TiO_2: effect of operational parameters, J. Hazard. Mater. 153 (2008) 1235–1239.
[30] J.-M. Herrmann, Water treatment by heterogeneous photocatalysis, in: F. Jansen, R.A. van Santen (Eds.), Environmental Catalysis, Catalytic Science Series, vol. 1, Imperial College Press, London, 1999 , pp. 171–194 (Chapter 9).
[31] N. Serpone, E. Pelizzetti (Eds.), Photocatalysis: Fundamentals and Applications,, Wiley/Interscience, New York, 1989.
[32] D.M. Blake, Bibliography of Work on the Photocatalytic Removal of Hazardous Compounds from Water and Air, NREL/TP-430-22197, National Renewable Energy Laboratory, Golden Co., 1997.
[33] C.-C. Chen, Degradation pathways of ethyl violet by photocatalytic reaction with ZnO dispersions, J. Mol. Catal. A: Chem. 264 (2007) 82–92.
[34] F.D. Mai, C.C. Chen, J.L. Chen, S.C. Liu, Photodegradation of methyl green using visible irradiation in ZnO suspensions: determination of the reaction pathway and identification of intermediates by a high-performance liquid Chromatography-photodiode array-electrospray ionization-mass spectrometry method, J. Chromatogr. A 1189 (2008) 355–365.
[35] K.M. Parida, S.S. Dash, D.P. Das, Physico-chemical characterization and photocatalytic activity of zinc oxide prepared by various methods, J.Colloid Interface Sci. 298 (2006) 787–793.
[36] M. Rezapour, N. Talebian, Comparison of structural, optical properties and photocatalytic activity of ZnO with different morphologies: effect of synthesis methods and reaction media, Mater. Chem. Phys. 129 (2011) 249–255.
[37] D.L. Liao, C.A. Badour, B.Q. Liao, Preparation of nanosized TiO_2/ZnO composite catalyst and its photocatalytic activity for degradation of methyl orange, J. Photochem. Photobiol. A 194 (2008) 11–19.
[38] S. Chakrabarti, B. Chaudhuri, S. Bhattacharjee, P. Das, B.K. Dutta, Degradation mechanism and kinetic model for photocatalytic oxidation of PVC–ZnO composite film in presence of a sensitizing dye and UV radiation, J. Hazard. Mater. 154 (2008) 230–236.
[39] B.D. Cullity, Elements of X-ray Diffraction, Edison-Wesley Publishing Company, Inc., 1978.
[40] R.W.G. Wyckoff, Crystal Structures, vol. 1, Interscience Publishers, New York, 1958.
[41] S.C. Abrahams, J. Bernstei, Remeasurement of structure of hexagonal ZnO, Acta Crystallogr. B-Struct. Crystallogr. Cryst. Chem. B 25 (1969) 1233–1238.
[42] Powder Diffraction File Release 2000, PDF Maintenance 6.0, International Center for Diffraction Data, Pennsylvania, 2000.
[43] R. Ghosh, D. Basak, Effect of substrate-induced strain on the structural electrical, and optical properties of polycrystalline ZnO thin films, J. Appl. Phys. 96 (2004) 2689–2693.
[44] S. Sakthivel, S.U. Geissen, D.W. Bahnemann, V. Murugesan, A. Vogelpohl, Enhancement of photocatalytic activity by semiconductor heterojunctions: α-Fe_2O_3 WO_3 and CdS deposited on ZnO, J. Photochem. Photobiol. A: Chem. 148 (2002) 283–293.
[45] Y. Liu, M. Zhong, G. Shan, Y. Li, B. Huang, G. Yang, Biocompatible ZnO/Au nanocomposites for ultrasensitive DNA detection using resonance Raman scattering, J. Phys. Chem. B112 (2008) 6484–6489.
[46] R. Konenkamp, R.C. Word, M. Godinez, Electroluminescence in nanoporous TiO_2 solid-state heterojunctions, Nanotechnology 17 (2006) 1858–1861.
[47] Y. Shimizu, E. Kanazawa, Y. Takao, M. Egashira, Modification of H_2-sensitive breakdown voltages of SnO_2 varistors with noble metals, Sens. Actuators B 52 (1998) 38–44.
[48] M.R. Hoffmann, S.T. Martin, W. Choi, D.W. Bahnemann, Environmental applications of semiconductor photocatalysis, Chem. Rev. 95 (1995) 69–96.
[49] D. Beydoun, R. Amal, G. Low, S. McEvoy, Role of nanoparticles in photocatalysis, J. Nanoparticle Res. 1 (1999) 439–458.
[50] Y. Xu, M.A.A. Schoonen, The absolute energy positions of conduction and valence bands of selected semiconducting minerals, Am. Miner. 85 (2000) 543–548.